Taylor & Francis
Taylor & Francis Group

Modelling the spatiotemporal dynamics of chemovirotherapy cancer treatment

Joseph Malinzi[a], Amina Eladdadi[b] and Precious Sibanda[c]

[a]Department of Mathematics and Applied Mathematics, University of Pretoria, Hatfield, South Africa; [b]Department of Mathematics, The College of Saint Rose, Albany, New York, USA; [c]School of Mathematics, Statistics, and Computer Science, University of KwaZulu Natal, Scottsville, South Africa

ABSTRACT

Chemovirotherapy is a combination therapy with chemotherapy and oncolytic viruses. It is gaining more interest and attracting more attention in the clinical setting due to its effective therapy and potential synergistic interactions against cancer. In this paper, we develop and analyse a mathematical model in the form of parabolic nonlinear partial differential equations to investigate the spatiotemporal dynamics of tumour cells under chemovirotherapy treatment. The proposed model consists of uninfected and infected tumour cells, a free virus, and a chemotherapeutic drug. The analysis of the model is carried out for both the temporal and spatiotemporal cases. Travelling wave solutions to the spatiotemporal model are used to determine the minimum wave speed of tumour invasion. A sensitivity analysis is performed on the model parameters to establish the key parameters that promote cancer remission during chemovirotherapy treatment. Model analysis of the temporal model suggests that virus burst size and virus infection rate determine the success of the virotherapy treatment, whereas travelling wave solutions to the spatiotemporal model show that tumour diffusivity and growth rate are critical during chemovirotherapy. Simulation results reveal that chemovirotherapy is more effective and a good alternative to either chemotherapy or virotherapy, which is in agreement with the recent experimental studies.

1. Introduction

Current cancer treatments involve combination therapies such as radioimmunotherapy [29, 58], radiovirotherapy [15, 59], and immunotherapy combined with targeted therapies [23, 41, 63], to name but a few. Presently, despite aggressive treatments including combination therapies, most cancers often recur due to their resistance to conventional therapies and limitations to effective therapies [60]. Recently, chemovirotherapy, a combination therapy with chemotherapy and oncolytic viruses, has gained increasing significance in the clinical setting. The essence of using chemovirotherapy is that oncolytic viruses directly lyse tumour cells or deliver genes that make them more susceptible to chemotherapeutic

---

CONTACT Joseph Malinzi ✉ josephmalinzi@aims.ac.za; Amina Eladdadi ✉ eladdadi@gmail.com; Precious Sibanda ✉ sibandap@ukzn.ac.za

drugs. In fact, many studies have concluded that the combination of oncolytic viruses with chemotherapy acts synergistically mainly because they are mediated by different pathways [1, 3, 52].

Numerous experimental studies have shown that, with the right combination of oncolytic viruses and standard cytotoxic chemotherapy agents, synergistic interactions occur resulting in enhanced therapeutic effects not attainable by either therapy alone [6, 43, 45, 49]. Chemovirotherapy has been experimentally and clinically tested for the treatment of some cancers such as malignant gliomas [3, 61], lymphoma [62], lung cancers [23], and metastatic breast cancer [12]. The study by Alonso et al. [3] showed that the combination of an oncolytic adenovirus (ICOVIR-5), with either everolimus (RAD001) or temozolomide (TMZ) resulted in an enhanced increase in the anti-glioma effect *in vitro* and *in vivo* glioma xenograft model. They concluded that the animals' median survival rate has increased by 20–40% and that they remained disease free beyond 90 days after treatment. Another experimental study on malignant glioma by Ulasov et al. [61] suggested that virotherapy and temozolomide chemotherapy, when combined, are able to eradicate malignant glioma. Their results showed that 90% of the treated mice survived beyond the 100 days' mark after being treated. In [62], Ungerechts et al. examined the synergy between a reprogrammed oncolytic virus and two chemotherapeutics in the mantle cell lymphoma (MCL). They investigated the efficacy of different regimens of a reprogrammed measles virus into an oncolytic virus in combination with two chemotherapeutics, fludarabine and cyclophosphamide (CPA) approved for treatment of lymphoma in an MCL xenograft model. Their study showed that CPA administration before virotherapy enhanced oncolytic efficacy. They concluded that a three 23-day courses of triple sequential treatment with CPA, virus and fludarabine treatment resulted in complete regression of the xenografts.

A recent experimental study by Gomez-Gutierrez et al. [23] showed that the chemotherapeutic drug (TMZ) enhances virotherapy in three lung cancer cell lines, concluding that combined therapy of the oncolytic adenovirus (adeAdhz60) and TMZ has a synergistic killing effect *in vitro*. In [12], Cody et al. presented a summary of oncolytic virotherapy strategies that have been used in a number of combinatorial therapeutic strategies to increase their effectiveness against breast cancer. They particularly reviewed the recent studies in which virotherapy has been combined with chemotherapeutic agents to target metastatic breast cancer. They communicated that all of these studies concluded that the antitumour efficacy of oncolytic viruses can be enhanced by chemotherapeutics agents. In addition, they discussed the challenges facing oncolytic virotherapy of metastatic breast cancer such as enhancing systemic delivery, promoting efficient intratumoral spread (overcoming matrix barriers, diffusion gradients, and poor viral replication), and limiting the antiviral immune response.

In [6], Binz and Ulrich gave a thorough and up-to-date review on the clinical studies in which the concepts of chemotherapy and virotherapy have been combined. They stated that phase II/III clinical trials on combining the adenovirus H101 with the chemotherapeutic drug cisplatin and 5-fluorouracil showed a 40% improvement compared to chemotherapy alone for the treatment of patients with head and neck cancer. They also communicated that these clinical studies have led to an early classification of chemovirotherapeutic combination regimens. In 2005, China approved adenovirus Ad-H101 for the treatment of head and neck cancers after phase III clinical trials showed a higher response rate for Ad-H101

combined with 5-fluorouracil (79–72%) compared to chemotherapy alone (40%) [21]. Ad-H101 became the first oncolytic virus to be approved for the treatment of human cancers. Ten years later, in 2015, the U.S. Food and Drug Administration approved Imlygic$^{\circledR}$ (talimogene laherparepvec), a genetically modified live oncolytic herpes virus therapy, as first oncolytic virotherapy for the treatment of melanoma lesions in the skin and lymph nodes [17, 18]. Earlier this year, it was also approved in Europe for some inoperable melanomas [30]. Most of these (and other studies not mentioned in this paper) have validated the general principle that oncolytic virotherapy could be harnessed as a component of a multi-modality cancer therapy.

Despite a large body of experimental and clinical work on oncolytic virus therapy, the mechanism of action of chemovirotherapy is still not well understood. Primarily, this is due to the complexity and the high non-linearity of the dynamics between tumour cells, oncolytic viruses, and their microenvironment [43, 45]. There is increasing evidence that mathematical models can be helpful in investigating the interactions between tumour cells and viruses. Indeed, various yet limited, mathematical models of oncolytic virus therapies have been developed to examine the emerging properties of these dynamics, suggest optimal treatment strategies as well as to inform the design of new experiments. For a comprehensive review on mathematical models of virotherapy, the reader is referred to excellent papers, reviews, and the references therein in [14, 20, 25, 26, 28, 66–69]. Here, we restrict our literature review to few key papers in modelling virotherapy treatments that have motivated the formulation of our model.

Tian [57] presented a basic mathematical model in the form of ordinary differential equations (ODEs), for virotherapy treatment which incorporated virus burst size. This mathematical model was based on an earlier basic virotherapy models of Wodarz and Komarova [70]. Tian concluded that besides the virus type, the burst size of an oncolytic virus and the tumour size determine the outcome of oncolytic treatment. Crivelli et al. [13] in an analysis of the cell cycle-specific activity of viruses noted that intracellular viral replication and the virus-tumour cells fusion are among the parameters that substantially impact the outcome of virotherapy. These parameters are equivalent to burst size and viral infection rate in our model.

In [36], Malinzi et al. presented a mathematical model to describe the interactions of the tumour-immune-virus dynamics. Their model included local kinetic interaction terms of the tumour and immune cells and a modified functional immune response to account for the saturation of immune cells in a tumour. The results from the study showed that the main virotherapy treatment properties were tumour cell movement and local kinetic interaction terms such as tumour growth and death rates. Unlike Malinzi et al. [36] who examined a one-dimensional spatial domain, in this paper we consider a three-dimensional spatial tumour domain, under the assumption of radial symmetry, thus providing for more realistic tumour geometry. Also, it is important to note that the immune system plays a very important role in tumour cells eradication from body tissue [16, 33, 39, 40]. We, however, for the sake of model tractability, do not consider immune cell interactions.

In this paper, we extend the growing literature on tumour virotherapy models by presenting a mathematical model of chemovirotherapy which builds upon those presented by Tian [57] and Malinzi et al. [36]. To this end, we develop and analyse a mathematical model which combines chemotherapy and virotherapy treatments. The model includes uninfected and infected tumour cells, free virus particles, and chemotherapeutic drug. The

aim is to investigate the spatiotemporal distribution of tumour cells and viruses as well as to determine the outcome of chemovirotherapy treatment. Moreover, through travelling wave solutions, numerical simulations, and sensitivity analysis, we intend to establish the key parameters that promote cancer remission during chemovirotherapy treatment.

This paper is organized as follows. In Section 2, we introduce the mathematical model, define the initial and boundary conditions, and re-scale the model. In Section 3, we set the baseline values for the parameters for simulating the model. In Section 4, we present the temporal model analysis and simulations. In Section 5, we determine travelling wave solutions to the spatiotemporal model and simulate the model in the cases of no treatment, chemotherapy, virotherapy, and chemovirotherapy. In Section 6, we perform a sensitivity analysis on the model parameters to determine which parameters have the greatest impact on model outcomes. The conclusion and discussion are presented in Section 7.

2. Mathematical model

2.1. Model construction

In this section, we devise a mathematical model that describes an avascular solid tumour growth under chemotherapy and virotherapy treatments in spherical coordinates under the assumption of radial symmetry. We consider an avascular tumour, with a necrotic core containing dead cells with a radius L_0, in a radially geometric setting with a fixed radius L. We consider a tumour nodule that has grown to its maximum size of about 1–3 mm diameter [40] and just prior to angiogenesis, an assumption necessary for clinical intervention. We model the movement of cells using the Kolmogorov equation [31], a linear diffusion model used for simulating cell movement. The variables used to describe the tumour progress and its interaction with the oncolytic virus and chemotherapy are:

- $U(r, t)$: uninfected tumour density in cells per mm^3
- $I(r, t)$: infected tumour cell density in cells per mm^3
- $V(r, t)$: free virus density in virions per mm^3
- $C(r, t)$: concentration of a chemotherapeutic agent in grams per millilitre (g/ml)

where $r \in [0, L]$ is the radius of the tumour at a time $t \in [0, \infty)$. Figure 1 depicts the interactions between tumour cells, virus, and a chemotherapeutic drug.

Tumour density, U(r, t), and I(r, t)

The following assumptions are made in order to model the evolution of a tumour over time and in space:

- The tumour is considered to grow logistically at an intrinsic rate α per day and its carrying capacity K is taken to be 10^6 cells [40].
- The infected tumour density, $I(r, t)$, increases as the oncolytic viruses multiply in the uninfected tumour cells and burst.
- Virus infection of the tumour is considered to be of Michaelis–Menten form [64].
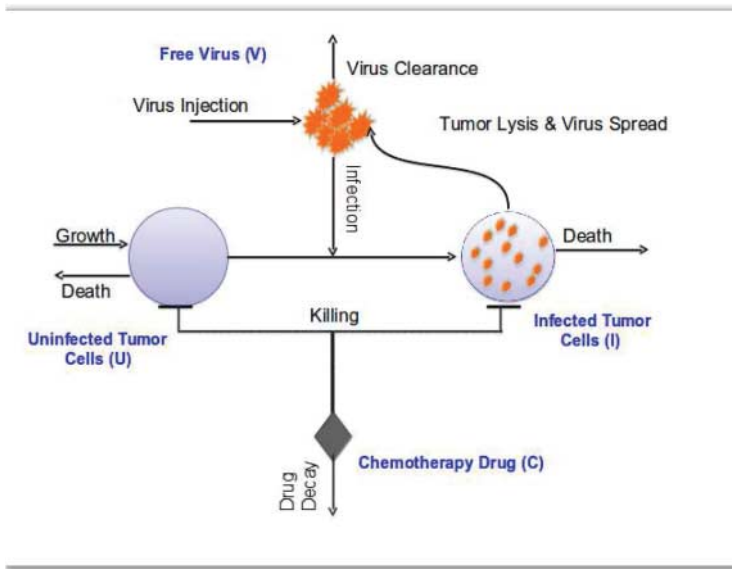
Figure 1. Diagram of the tumour–virus–chemotherapy interactions. Uninfected tumour cells are infected upon entry of a free virus. Infected cells undergo lysis resulting in release of free viruses. Chemotherapy drug, injected directly in the body tissue, kills both the uninfected and infected tumour cells.

- The tumour–virus interaction is one to one, that is, one virus infects one tumour cell which later multiplies into infected tumour cells [57].
- The chemotherapeutic drug is administered as a single bolus and its concentration in the blood stream decays exponentially [55].
- The drug kills the tumour cells in a concentration-dependent manner [19], that is, the drug cytotoxicity increases with increasing drug concentration, asymptotically approaching its maximum.

The uninfected and infected tumour cell densities are governed by the following reaction–diffusion equations:

$$\frac{\partial U}{\partial t} = \underbrace{D_1 \frac{1}{r^2} \frac{\partial}{\partial r}\left[r^2 \frac{\partial U}{\partial r}\right]}_{\text{Diffusion}} + \underbrace{\alpha U\left(1 - \frac{U+I}{K}\right)}_{\text{Tumour growth}} - \underbrace{\frac{\beta UV}{K_u + U}}_{\text{Loss of } U \text{ due to infection}} - \underbrace{\frac{\delta_0 UC}{K_c + C}}_{\text{Drug response}} , \quad (1)$$

$$\frac{\partial I}{\partial t} = \underbrace{D_2 \frac{1}{r^2} \frac{\partial}{\partial r}\left[r^2 \frac{\partial I}{\partial r}\right]}_{\text{Diffusion}} + \underbrace{\frac{\beta UV}{K_u + U}}_{\text{Gain of I due to infection}} - \underbrace{\frac{\delta_1 IC}{K_c + C}}_{\text{Drug response}} - \underbrace{\delta I}_{\text{Death of infected tumour cells}} .$$

$$(2)$$

In Equations (1) and (2), the terms $D_1(1/r^2)(\partial/\partial r)[r^2(\partial U/\partial r)]$ and $D_2(1/r^2)(\partial/\partial r)[r^2(\partial I/\partial r)]$, respectively, represent diffusion in spherical coordinates, under radial symmetry, for the uninfected and infected tumour cells to model tumour movement. D_1 and

D_2 are, respectively, the uninfected and infected tumour diffusion constants. The second term $\alpha U(1 - (U + I)/K)$ represents tumour progression, where α is the intrinsic tumour growth rate and K is the carrying capacity. The third term $-\beta UV/(K_u + U)$ models infection of tumour cells by the virus, where β is the infection rate measured per day per number of cells. It is of Michaelis–Menten form to account for saturation in the virus proliferation [36, 64]. The terms $-\delta_0 UC/(K_c + C)$ and $-\delta_1 IC/(K_c + C)$, respectively, represent chemotherapeutic drug responses to uninfected and infected tumour cells where δ_0 and δ_1 are lysis-induced rates measured per day. K_u and K_c are, respectively, Michaelis–Menten constants which relate to lysis rates when the virus and the drug are half-maximal. The term $\beta UV/(K_u + U)$, in Equation (2), describes a gain in infected tumour cells due to infection by the virus. The last term in Equation (2), that is $-\delta I$, represents the death of infected tumour cells where δ is the death rate.

Virus density, $V(r, t)$

Virus production is dependent on its burst size, that is, the larger the burst size, the higher the number of viruses produced [57]. Virus production is taken to be $b\delta I$, where b is the virus burst size measured per day and δ is the infected tumour cell death rate measured per day [57]. The virus gets deactivated in body tissue at a rate γ per day. The non-linear differential equation describing the virus density is given by:

$$\frac{\partial V}{\partial t} = D_3 \underbrace{\frac{1}{r^2}\frac{\partial}{\partial r}\left[r^2 \frac{\partial V}{\partial r}\right]}_{\text{Diffusion}} + \underbrace{b\delta I}_{\text{Virus production}} - \underbrace{\frac{\beta UV}{K_u + U}}_{\text{Loss of } V \text{due to infection}} - \underbrace{\gamma V}_{\text{Virus deactivation}}. \quad (3)$$

In Equation (3), the term $D_3(1/r^2)(\partial/\partial r)[r^2(\partial V/\partial r)]$ represents virus diffusion, where D_3 is the virus diffusion constant. Viruses reproduce by engulfing tumour cells and bursting thus releasing other copies. The term $-\beta UV/(K_u + U)$ describes loss of free virus due to infection of the uninfected tumour cells. The last term in Equation (3), that is $-\gamma I$, represents virus decay from body tissue.

Drug density, $C(r, t)$

Drug penetration into the tumour is modelled using reaction–diffusion. The drug density is governed by the following reaction diffusion equation:

$$\frac{\partial C}{\partial t} = D_4 \underbrace{\frac{1}{r^2}\frac{\partial}{\partial r}\left[r^2 \frac{\partial C}{\partial r}\right]}_{\text{Diffusion}} + \underbrace{C_b(t)}_{\text{Drug plasma level}} - \underbrace{\mu C}_{\text{Drug decay}}. \quad (4)$$

Similarly, in Equation (4) the term $D_4(1/r^2)(\partial/\partial r)[r^2(\partial C/\partial r)]$ represents chemotherapeutic drug diffusion, where D_4 is the drug diffusion coefficient, $C_b(t) = \psi\, e^{(-kt)}$ is the prescribed drug plasma level in the blood stream, and $-\mu C$ is the natural drug concentration decay, where μ is the rate of decay. The constant ψ is the rate of drug infusion and k relates to the chemotherapy drug half life, $T_{1/2}$, which is roughly one day [50], and is given by $k = \ln 2/T_{1/2}$. Figure 1 displays the tumour–virus–chemotherapy interactions and Table 1 gives a summary of all the parameter descriptions, their baseline values, units, and sources.

Table 1. A summary of the parameter descriptions, their baseline value ranges, and their sources.

Parameter	Description	Value/units and units	References
$D_i, i = 1, 2 \ldots 4$	Cell diffusion coefficients	10^{-3}–10^{-6} cm^2 day^{-1}	[48]
α	Intrinsic tumour growth rate	0.1–0.3 day^{-1}	[54]
K	Tumour carrying capacity	10^5–10^9 number of cells	[54]
β	Virus infection rate of U by V	0.001 day^{-1} number of cells^{-1}	[5]
δ_0	Lysis-induced rate of U by C	0.005 day^{-1}	[47]
δ_1	Lysis-induced rate of I by C	0.006 day^{-1}	[1, 7, 44]
K_u	Michaelis–Menten constant	10^5 g/ml	[27]
K_c	Michaelis–Menten constant	10^5 g/ml	[27]
b	Virus burst size	2–1000 day^{-1}	[1, 7, 44]
δ	Infected tumour cell death	0.5115 day^{-1}	[4, 5]
γ	Virus deactivation rate	0.001–0.1 day^{-1}	[4, 9]
ψ	Rate of drug infusion	20–200 ml day^{-1}	[1, 7, 44]
k	Drug half life constant	0.01–0.9 day^{-1}	[50]
μ	Rate of drug decay	4.17 day^{-1}	[1, 7, 44]
ρ	Tumour permeability	0.01 g^{-1}	[32]

Note: est: estimated.

2.2. Initial and boundary conditions

This section gives an account for the choice of the initial and boundary conditions for the model. A tumour nodule comprises three layers: a necrotic core containing dead cells, and quiescent and proliferating zones comprising living cells [11]. We therefore consider the uninfected tumour density in the necrotic core to be zero and that it increases outwards, that is, in the quiescent and proliferating zones [36]. Initially, the drug and virus densities are considered to lie on the sheath of the tumour in small concentrations. This is because the boundary in which we investigate the tumour–drug–virus interactions is the tumour sheath. We consider no flux boundary conditions for all cell concentrations at $r = 0$, the centre of the tumour, because it contains dead cells. At the boundary $r = L$, we consider no flux conditions for the infected and uninfected tumour cells since the tumour is considered to be at avascular growth stage with no small amounts of cells escaping through the tumour sheath to spread into the surrounding tissue [2, 40]. Zero flux boundary conditions are assumed for the virus density, at $r = L$, because of the cancellation of flux from inside and outside the tumour [46]. The chemotherapeutic drug diffuses into the tumour through the outside tumour boundary $r = L$ whose permeability is denoted as ρ and the virus density at the boundary is determined by the tumour–virus interactions. With these assumptions we close off the system (1)–(4) with the following initial and boundary conditions:

$$U(r, 0) = \begin{cases} 0, & 0 \leq r \leq L_0, \\ U_0(1 - e^{-100(r-L_0)^2}), & L_0 \leq r \leq L, \end{cases}$$

$$I(r, 0) = 0, \quad r \in [0, L],$$

$$V(r, 0) = \begin{cases} V_0, & r = L, \\ 0, & \text{elsewhere}, \end{cases} \tag{5}$$

$$C(r, 0) = \begin{cases} C_0, & r = L, \\ 0, & \text{elsewhere}, \end{cases}$$

$$\left.\frac{\partial U}{\partial r}\right|_{r=0} = \left.\frac{\partial I}{\partial r}\right|_{r=0} = \left.\frac{\partial V}{\partial r}\right|_{r=0} = \left.\frac{\partial C}{\partial r}\right|_{r=0} = 0,$$

$$\left.\frac{\partial U}{\partial r}\right|_{r=L} = \left.\frac{\partial I}{\partial r}\right|_{r=L} = 0, \quad \left.D_3\frac{\partial V}{\partial r}\right|_{r=L} = 0, \quad \left.D_4\frac{\partial C}{\partial r} + \rho C\right|_{r=L} = 0, \tag{6}$$

where L_0 is the radius of the necrotic core.

2.3. Model re-scaling

The system (1)–(4) is re-scaled by setting $\bar{U} = U/K$, $\bar{I} = I/K$, $\bar{V} = V/V_0$, and $\bar{C} = C/C_0$ with $\bar{t} = t/t_0$ and $\bar{r} = r/r_0$ where U_0, I_0, V_0, and C_0 are initial cell concentrations and the space variable, r, is re-scaled relative to the length of the region under study, that is, $r_0 = 1$ [40]. The parameters become

$$\phi_i = D_i t_0, \quad i = 1, 2, 3, 4, \quad \bar{\alpha} = \alpha t_0, \quad \bar{\beta} = \frac{\beta V_0 t_0}{U_0}, \quad \bar{\delta}_0 = \delta_0 C_0 t_0, \quad \bar{K}_u = \frac{K_u}{U_0},$$

$$\bar{K}_c = \frac{K_c}{C_0}, \quad \bar{\delta}_1 = \delta_1 C_0 t_0, \quad \bar{b} = \frac{bK}{V_0}, \quad \bar{\gamma} = \gamma t_0, \quad \bar{\psi} = \frac{\psi t_0}{C_0}, \quad \bar{\mu} = \mu t_0, \quad \phi_5 = \frac{D_4}{r_0}.$$

Dropping the bars for clarity and taking the necrotic core to be of radius 0.2 mm [22] gives a re-scaled model defined by the following parabolic system of non-linear reaction diffusion equations:

$$\frac{\partial U}{\partial t} = \phi_1 \frac{1}{r^2}\frac{\partial}{\partial r}\left[r^2\frac{\partial U}{\partial r}\right] + \alpha U(1 - U - I) - \frac{\beta UV}{K_u + U} - \frac{\delta_0 UC}{K_c + C}, \tag{7}$$

$$\frac{\partial I}{\partial t} = \phi_2 \frac{1}{r^2}\frac{\partial}{\partial r}\left[r^2\frac{\partial I}{\partial r}\right] + \frac{\beta UV}{K_u + U} - \frac{\delta_1 IC}{K_c + C} - \delta I, \tag{8}$$

$$\frac{\partial V}{\partial t} = \phi_3 \frac{1}{r^2}\frac{\partial}{\partial r}\left[r^2\frac{\partial V}{\partial r}\right] + bI - \frac{\beta UV}{K_u + U} - \gamma V, \tag{9}$$

$$\frac{\partial C}{\partial t} = \phi_4 \frac{1}{r^2}\frac{\partial}{\partial r}\left[r^2\frac{\partial C}{\partial r}\right] + C_b(t) - \mu C, \tag{10}$$

with the initial and boundary conditions (11) and (12).

$$U(r, 0) = \begin{cases} 0, & 0 \leq r \leq 0.2, \\ 1 - e^{(-100r - L_0)^2}, & 0.2 \leq r \leq 1, \end{cases}$$

$$I(r, 0) = 0, \quad r \in [0, 1],$$

$$V(r, 0) = \begin{cases} 1, & r = 1, \\ 0, & \text{elsewhere}, \end{cases} \tag{11}$$

$$C(r, 0) = \begin{cases} 1, & r = 1, \\ 0, & \text{elsewhere} \end{cases}$$

and

$$\frac{\partial U}{\partial r}\bigg|_{r=0} = \frac{\partial I}{\partial r}\bigg|_{r=0} = \frac{\partial V}{\partial r}\bigg|_{r=0} = \frac{\partial C}{\partial r}\bigg|_{r=0} = 0,$$

$$\frac{\partial U}{\partial r}\bigg|_{r=1} = \frac{\partial I}{\partial r}\bigg|_{r=1} = 0, \quad \phi_3\frac{\partial V}{\partial r} + \rho V\bigg|_{r=1} = 0, \quad \phi_5\frac{\partial C}{\partial r} + \rho C\bigg|_{r=1} = 0. \tag{12}$$

3. Parameter estimation and baseline values

To date, there is still no available longitudinal data for chemovirotherapy treatment. To simulate our model, we first determine the baseline parameter values from the literature that most correspond to available experimental chemotherapy, virotherapy data, and biological facts. A summary of the parameter descriptions along with their numerical values and references is given in Table 1.

3.1. Diffusion coefficients

The diffusion coefficients for the tumour, D_1 and D_2, were estimated using the formula, $D = 4R^2q$, where R and q are, respectively, the tumour radius and growth rate, discussed in Prigogine and Lefever [48]. These values are approximated to be $q = 0.1$–1 day^{-1} and $R = 4\,\mu$m. Therefore, D_1 and D_2 are approximated to be 10^{-6}–10^{-3} cm^2 day^{-1}. The virus diffusion coefficient, D_3, was estimated using Einstein's formula $D = \kappa T/(6\pi R\tau)$, where κ is Boltzmann's constant, T is the temperature, R is the radius of a virus cell, and τ is the viscosity coefficient of the medium [40]. The temperature and viscosity coefficients are known to be $T = 310$ K, and $\tau = \rho_{\text{water}}$. We consider the radius of the virus to be a fraction of that for the tumour. Therefore, $R = 1 - 4\,\mu$m. Virus diffusivity, D_3, is therefore approximated to be 10^{-5} cm^2 day^{-1}. Since the oncolytic virus is laboratory made to be injected into body tissue, the drug diffusion coefficient is considered to be in the same range as that of the virus.

3.2. Tumour growth and carrying capacity

The carrying capacity of the tumour is taken to be 10^6 cells per unit volume because a tumour nodule contains about 10^5–10^9 tumour cells [54]. The tumour growth rate was taken to be 0.26 day^{-1} because several experimental tumour growth models estimate it to be in the range of 0.1–1 [5].

3.3. Virus production and infection rate parameters

Viral burst size is the number of viruses released from each infected tumour cell. This alludes to the fact that virus emission leads to either cell lysis or cell death. The production of new viruses from infected tumour cells therefore occurs as a burst of a characteristic numbers of viruses, on time scales ranging from minutes to days [9]. Burst sizes for different viruses have a large range corresponding to their genus. The number of oncolytic viruses produced in a day is considered to be in the range 2–1000 [9]. The infected tumour cell death is estimated by Bajzer et al. [4] to be 0.5115 day^{-1}.

3.4. Chemotherapeutic drug parameters

The rate of drug infusion into body tissue is taken to be 20 mg/day since most cancers require high doses of treatment and the drug decay rate is estimated to be 4.17 mg/day, values which concur with cancer pharmacokinetic studies [1, 7, 44]. Since infected tumour cells multiplication is enhanced by the oncolytic virus replication, the tumour cells lysis is considered to be greater than that for uninfected tumour cells [47]. The half life of several chemotherapeutic drugs is one hour to a month [65]. Therefore, we estimate the value of k to be $k = \ln 2 / T_{1/2} = 0.01$ to 0.8.

To predict tumour cell densities at different time periods without the consideration of space, we first analyse and simulate the model without spatial dynamics which we present in the next section.

4. Temporal model analysis

In this section, we investigate the temporal model's phase space properties, present its asymptotics and stability, and run some simulations to support analytical findings. Without spatial effects the model, Equations (7)–(10) become:

$$\frac{dU}{dt} = \alpha U(1 - U - I) - \frac{\beta UV}{K_u + U} - \frac{\delta_0 UC}{K_c + C},\tag{13}$$

$$\frac{dI}{dt} = \frac{\beta UV}{K_u + U} - \frac{\delta_1 IC}{K_c + C} - \delta I,\tag{14}$$

$$\frac{dV}{dt} = bI - \frac{\beta UV}{K_u + U} - \gamma V,\tag{15}$$

$$\frac{dC}{dt} = C_b(t) - \mu C.\tag{16}$$

4.1. Phase space properties

The solutions to model (13)–(16) are cell densities and concentrations which would only make sense when they are positive quantities. It is important to first investigate solutions existence and show that trajectories which start non-negative remain non-negative and that the solutions never blow up.

Theorem 4.1:

(1) *There exists a unique positive solution to the temporal model* (13)–(16) *on some domain* $X = [0, b)$, $b > 0$.
(2) *The solutions to the model* (13)–(16) *are bounded from above and the trajectories evolve in an attracting region* $\mathbb{D} \in X$, *where*

$$\mathbb{D} = \left\{ (U, I, V, C) \in \mathbb{R}_+^4 \mid 0 \leq U + I \leq 1, \ 0 \leq V \leq \frac{b}{\gamma}, \ 0 \leq C \leq C^* \right\},$$

where C^* is the maximum value attained by the chemotherapeutic drug concentration.
(3) *The solutions to the model* (13)–(16) *are positive, bounded and defined for all $t \geq 0$.*

Proof: (1) Equation (16) is a first-order linear differential equation and can be solved using a suitable integrating factor to obtain

$$C(t) = \left(C_0 + \frac{\psi}{k-\mu}\right)e^{-\mu t} + \left(\frac{\psi}{\mu-k}\right)e^{-kt}, \quad k \neq \mu, \quad \lim_{t\to\infty} C(t) = 0. \quad (17)$$

For Equations (14)–(16), we use Theorem **A.4.** in [56] which is stated as follows:

Theorem: *Let* $\mathbb{R}_+^n = [0,\infty)$ *be the cone of non-negative vectors in* $\mathbb{R}^n$. *Let* $F : \mathbb{R}_+^{n+1} \to \mathbb{R}^n$ *be locally Lipschitz,*

$$F(t,x) = (F_1(t,x),\ldots F_n(t,x)), \quad x = (x_1,\ldots x_n),$$

and satisfy

$$F_j(t,x) \geq 0 \quad \text{whenever } t \geq 0, \ x \in \mathbb{R}_+^n, \ x_j = 0.$$

Then, for every $x^\circ \in \mathbb{R}_+^n$, *there exists a unique solution of* $x' = F(t,x)$, $x(0) = x^\circ$, *with values in* $\mathbb{R}_+^n$, *defined on some interval* $[0,b)$, $b > 0$.

The functions, $F(U,I,V)$ on the left of Equations (14)–(16) and their partial derivatives are continuous on $\mathbb{R}^4$ and
 (i) In (13), $F(I,V,C) \geq 0$ whenever $t \geq 0$, $(U,I,V) \in \mathbb{R}_+^n$, $U = 0$
 (ii) In (14), $F(U,V,C) \geq 0$ whenever $t \geq 0$, $(U,I,V) \in \mathbb{R}_+^n$, $I = 0$
 (iii) In (15), $F(U,I,C) \geq 0$ whenever $t \geq 0$, $(U,I,V) \in \mathbb{R}_+^n$, $V = 0$
 (iv) In (16), $F(U,I,V) \geq 0$ whenever $t \geq 0$, $(U,I,V) \in \mathbb{R}_+^n$, $C = 0$
(2) From Equations (13) and (14),

$$\frac{dU}{dt} + \frac{dI}{dt} = \alpha U(1 - (U+I)) - \frac{\delta_0 UC}{K_c + C} - \frac{\delta_1 IC}{K_c + C} - \delta_1 I$$

$$\leq \alpha(U+I)(1 - (U+I)). \text{ Let } U + I = W,$$

$$W(t) \leq \frac{1}{B e^{-\alpha t} + 1},$$

$$\sup_{t\in[0,b)} W(t) \leq 1,$$

where $B = (1 - W_0)/W_0$. From Equation (15),

$$\frac{dV}{dt} = bI - \frac{\beta UV}{K_u + U} - \gamma V \leq b - \gamma V, \quad (18)$$

$$V(t) \leq \frac{1 - V_0 e^{-\gamma t}}{b}, \quad (19)$$

$$\sup_{t\in[0,b)} V(t) \leq \frac{b}{\gamma}. \quad (20)$$

The solution to Equation (16) exponentially decreases with time provided that $k \geq \mu$ and the highest possible concentration, C^*, is $C(t_0)$, where

$$t_0 = \log \left[\frac{(\frac{\psi}{\mu - k} - C_0)}{\frac{\psi}{k - \mu}} \right].$$

(3) Since the bound of U, I, V, and C on $[0, b)$ is finite, then b must be infinite. ∎

Theorem 4.1 states that the solutions to the model (13)–(16) are positive and bounded. Thence the cell concentrations are biologically meaningful since body tissue can only contain a finite amount of cells. Equation (17) shows that with time the drug concentration is depleted from body tissue provided that k, a constant which relates to the drug half life, is greater than the rate of drug decay. We next determine the model equilibria and their stability to predict long-term behaviour of the model solutions.

4.2. Asymptotics and stability

In order to determine steady-state solutions of the model (13)–(16), the system equations are first transformed into an autonomous system of ODEs by letting $y = C_b(t) = \psi \, e^{-kt}$ such that $dC/dt = y - \mu C$ and $dy/dt = -ky$.

Theorem 4.2: *The model* (13)–(16) *has three biologically meaningful steady states; a tumour-free state where the tumour is eradicated from body tissue, that is,* $U = 0$, $I = 0$, $V = 0$, $C = 0$, $y = 0$, *which is unstable, a state where the tumour grows to maximum size, that is,* $U = 1$, $I = 0$, $V = 0$, $C = 0$, $y = 0$, *and a state where the tumour co-exist with the virus, that is,*

$$U = \frac{\delta \gamma K_u}{\beta(b - \delta) - \delta \gamma},$$

$$I = \frac{(\delta \gamma K_u - b\beta + \beta \delta + \delta \gamma)\alpha \gamma K_u}{(\alpha \gamma K_u + b\beta - \beta \delta - \delta \gamma)(\beta \delta + \delta \gamma - b\beta)}, \qquad (21)$$

$$V = \frac{(\delta \gamma K_u - b\beta + \beta \delta + \delta \gamma)\alpha(b - \delta)K_u}{(\alpha \gamma K_u + b\beta - \beta \delta - \delta \gamma)(\beta \delta - \delta \gamma - b\beta)},$$

$$C = 0, \quad y = 0$$

provided that $b\beta > \delta(\gamma K_u + \beta + \gamma)$ *and* $b > \delta$.

Proof: The characteristic polynomial of the Jacobian matrix evaluated at the tumour-free steady state has both positive and negative real roots, that is, $-\gamma, -\mu, -k, \alpha, -\delta$. This shows that the tumour-free state is unstable. ∎

The other states are either stable or unstable depending on the parameter values, mostly K_u, K_c, and β. Equation (21) shows that with time, except for the chemotherapeutic drug, all tumour densities co-exist in body tissue. High values of the virus burst size b and the virus infection rate β lead to lower tumour densities. Moreover, Theorem 4.2 biologically implies that without the consideration of space, the temporal model predicts that
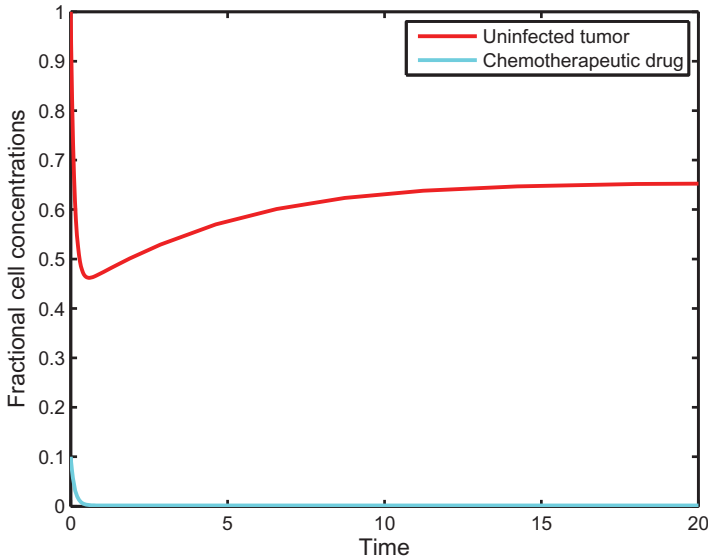
Figure 2. Simulations of the temporal model (13)–(16) for chemotherapy, that is $I = V = 0$, showing a variation of the fractional tumour and drug concentrations with time. The non-dimensional parameter values in Equation (22) were used. The plot shows the drug, as it gets depleted, reducing the tumour concentration.

the tumour may either co-exist with the virus in small concentrations or it may grow to its maximum size depending on several conditions as defined by the parameters in Equation (21).

4.3. Temporal model simulations

In this section, we present numerical simulations of the model (13)–(16) to support analytical findings and to predict changes in tumour size in response to either treatments, and to the combination of the chemotherapy with the virotherapy. The fourth-order Runge–Kutta method is used to discretise the system of equations. The dimensional values in Table 1 were re-scaled by taking $t_0 = 1/\delta$ to give the following non-dimensional parameter values:

$$\alpha = 0.4027, \quad \beta = 0.002, \quad \delta_0 = 9.76, \quad \delta_1 = 11.73, \quad \gamma = 0.002, \quad K_u = 0.01,$$

$$K_c = 0.01, \quad b = 10, \quad \gamma = 0.002, \quad \psi = 0.5865, \quad \mu = 8.13, \quad k = 0.1. \tag{22}$$

Initially, the tumour is assumed to have grown to maximum size to necessitate treatment. The fractional concentrations are therefore taken to be $U_0 = 1$, $I_0 = 0$, $V_0 = 0.1$, and $C_0 = 0.1$.

First, we simulate the model with either treatments, then chemotherapy and virotherapy treatments combined. In this simulation, one unit on the time scale represents two days, whereas one unit on the cell concentrations scale represents 10^6 number of cells. Figure 2 displays chemotherapy treatment with time. The simulation results show that after 40 days, although the tumour decreased to its steady states when the drug is depleted, it is not completely wiped out from the body tissue. Figure 3 shows the temporal variation of the tumour and virus concentrations using virotherapy. The simulation results show that
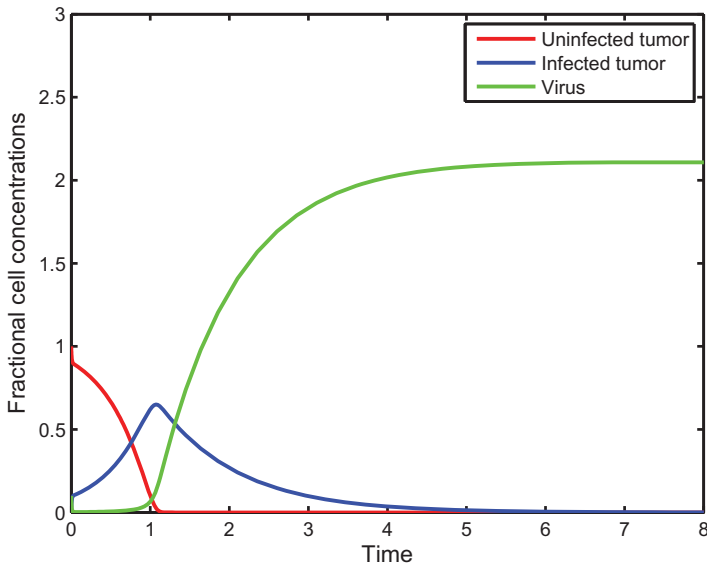
Figure 3. Simulations of the temporal model for virotherapy (13)–(16), that is $C = 0$, showing a variation of the fractional cell concentrations with time. The non-dimensional parameter values in Equation (22) were used. The simulation shows the virus infecting and lysing all tumour cells after 10 days.

it takes about two days for all tumour cells to be infected and about ten days for all the tumour cells to reduce to undetectable cell counts. Figure 4 depicts the case of the combination of chemotherapy and virotherapy. The simulation results show that it takes less than four days for all tumour cells to be infected and die out completely.

Biologically, these simulation results imply that the treatment of cancer with chemovirotherapy is more effective than chemotherapy and virotherapy alone, which is in accordance with some experimental studies [60, 71]. These results also show that it would take a shorter time period to clear all tumour cells from the body tissue which is in line with the experimental study by Weber et al. [66].

5. Spatiotemporal model analysis

In this section, we analyse the full model (7)–(10) to investigate the spatial dynamics of the cell densities. First, in one dimension and with constant drug infusion, we employ a technique used by Maidana and Yang [34] and Chahrazed et al. [10] to determine the minimum wave speed of the travelling wave solutions to the model (7)–(10). In doing this, we seek to determine the parameters which define the minimum speed of tumour invasion, thus determining the factors which characterize the potential with which a tumour invades body tissue. We later present results from numerical simulations of the model (7)–(10).

5.1. Travelling wave analysis

Using the transformation $\zeta = r - ct$, where c is the propagation speed, Equations (7)–(10), in one dimension, are transformed to:

$$\frac{\mathrm{d}^2 U}{\mathrm{d}\zeta^2} + G_1(U, I, V, C)\frac{\mathrm{d}U}{\mathrm{d}\zeta} + F_1(U, I, V, C) = 0, \tag{23}$$
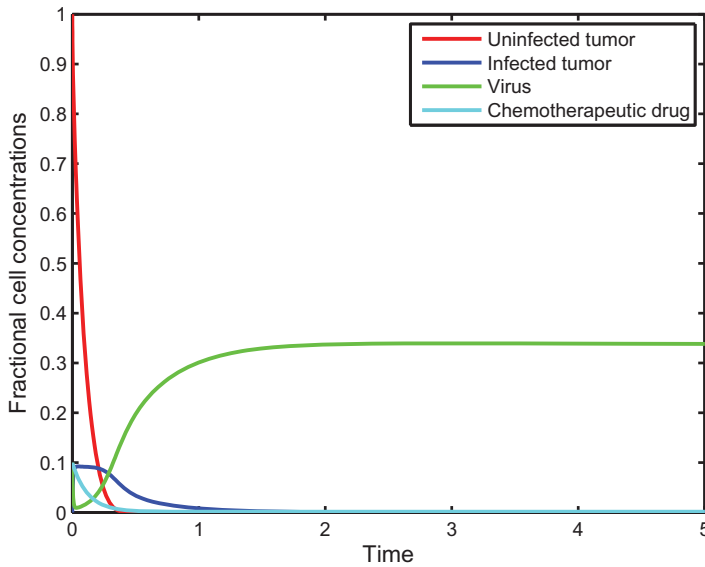
Figure 4. Simulations of the temporal model (13)–(16) for the combination of chemotherapy and virotherapy treatments. The plots are a variation of the fractional cell concentrations with time. The non-dimensional parameter values in Equation (22) were used. The simulations are similar to those with virotherapy treatment although it would take less time for tumour depletion from body tissue.

$$\frac{d^2 I}{d\zeta^2} + G_2(U, I, V, C)\frac{dI}{d\zeta} + F_2(U, I, V, C) = 0, \tag{24}$$

$$\frac{d^2 V}{d\zeta^2} + G_3(U, I, V, C)\frac{dV}{d\zeta} + F_3(U, I, V, C) = 0, \tag{25}$$

$$\frac{d^2 C}{d\zeta^2} + G_4(U, I, V, C)\frac{dC}{d\zeta} + F_4(U, I, V, C) = 0, \tag{26}$$

where

$$G_1 = \frac{c}{\phi_1}, \quad F_1 = c_1 U \left(\alpha(1 - U - I) - \frac{\beta V}{K_u + U} - \frac{\delta_0 C}{K_c + C} \right),$$

$$G_2 = \frac{c}{\bar{\phi}_2}, \quad F_2 = c_2 I \left(\frac{\beta U V}{I(K_u + U)} - \frac{\delta_1 C}{K_c + C} - \delta \right),$$

$$G_3 = \frac{c}{\bar{\phi}_3}, \quad F_3 = c_3 V \left(\frac{bI}{V} - \frac{\beta U}{K_u + U} - \gamma \right),$$

$$G_4 = \frac{c}{\bar{\phi}_4}, \quad F_4 = c_4 C \left(\frac{\psi}{C} - \mu \right),$$

where $c_i = 1/\bar{\phi}_i, i = 1, 2, 3, 4.$

By letting $y_1 = dU/d\zeta$, $y_2 = dI/d\zeta$, $y_3 = dV/d\zeta$, and $y_4 = dC/d\zeta$, Equations (23)–(26) are transformed into a system of first-order differential equations:

$$\frac{dY}{d\zeta} = f(Y) \quad \text{where } Y = \begin{pmatrix} y_1 \\ U \\ y_2 \\ I \\ y_3 \\ V \\ y_4 \\ C \end{pmatrix} \in \mathbb{R}^8 \tag{27}$$

and

$$f(Y) = \begin{pmatrix} -G_1 y_1 - F_1 \\ y_1 \\ -G_2 y_2 - F_2 \\ y_2 \\ -G_3 y_3 - F_3 \\ y_3 \\ -G_4 y_4 - F_4 \\ y_4 \end{pmatrix}, \tag{28}$$

with boundary conditions

$$\lim_{\zeta \to -\infty} (y_1, U, y_2, I, y_3, V, y_4, C) = Y^1,$$

and

$$\lim_{\zeta \to +\infty} (y_1, U, y_2, I, y_3, V, y_4, C) = Y^2,$$

where Y^1 and Y^2 correspond to the equilibrium solutions of Equation (28). Y^1 is the tumour-free equilibrium and Y^2 is the equilibrium solution where either the tumour grows to maximum size or where all cell concentrations co-exist. A travelling wave solution is the trajectory that joins Y^1 and Y^2. The tumour-free equilibrium must therefore not oscillate, that is a trajectory leaving Y^1 must move to the stable equilibrium. Consequently, in determining the minimum wave speed the eigenvalues of the Jacobian matrix evaluated about Y^1 must have real values. The eigenvalues, λ_i, $i = 1, 2, \ldots 8$, of the Jacobian matrix of Equation (28) are:

$$\lambda_{1,2} = -\frac{c \pm \sqrt{c^2 + 4\mu\phi_4}}{2\phi_4}, \tag{29}$$

$$\lambda_{3,4} = -\frac{c \pm \sqrt{c^2 + 4\gamma\phi_3}}{2\phi_3}, \tag{30}$$

$$\lambda_{5,6} - \frac{c \pm \sqrt{c^2 + 4\delta\phi_2}}{2\phi_2}, \tag{31}$$

$$\lambda_{7,8} = -\frac{c \pm \sqrt{c^2 - 4\alpha\phi_1}}{2\phi_1}. \tag{32}$$

The eigenvalues λ_1 to λ_6 in Equations (29)–(31) are real. Equation (32) therefore determines the minimum wave speed. This is obtained by setting $\sqrt{c^2 - 4\alpha\phi_1} = 0$ which gives $c = 2\sqrt{\alpha\phi_1}$. This speed highlights the parameters which are critical during chemovirotherapy treatment. These parameters are tumour diffusivity and growth rate.

5.2. Spatiotemporal model simulations

We now present numerical simulations of the model (7)–(10) with space to investigate tumour cell distributions in space with time. The multi-domain monomial based collocation method [42] and pdepe [53], a finite element-based method in Matlab, are used to determine the numerical solutions. In re-scaling the spatiotemporal model, we take $t_0 = 1/D_1$ which gives rise to the following non-dimensional parameter values:

$$\phi_1 = 1, \quad \phi_2 = 0.01, \quad \phi_3 = 0.01, \quad \phi_4 = 0.01, \quad \rho = 0.01,$$
$$\alpha = 206, \quad \beta = 511, \quad \delta_0 = 5 \times 10^6, \quad \delta_1 = 6 \times 10^6, \quad K_u = 0.1,$$
$$K_c = 0.1, \quad \delta = 0.005, \quad b = 3, \quad \gamma = 0.002, \quad \psi = 0.0050, \quad \mu = 4160, \quad k = 0.1. \tag{33}$$

We simulate the model in the following cases: no treatment, chemotherapy alone, virotherapy alone, and lastly combination of chemotherapy and virotherapy as described in the following sections.

5.2.1. No treatment

To investigate the efficacy of each treatment and their combination, we first simulate Equation (7) which models tumour growth without any form of treatment, that is $C = V = I = 0$. Figure 5 illustrates the initial tumour distributions. Simulation results show that the tumour density is zero in the necrotic core (i.e. $0 \leq r \leq 0.2$) and increases towards the tumour sheath. The infected tumour density is zero throughout the tissue since there was no virotherapy treatment. Figure 6 shows the distribution of tumour cells in the tissue without any form of treatment. The simulation results indicate that tumour density increases with time. This can be seen from Figure 6 (a,b), where after 25 days the fractional tumour density rose to 0.998×10^6 cells per unit volume from 0.84×10^6 cells per unit volume, which is about 16% increase.

Next, we simulate each of the chemotherapy and virotherapy treatments separately to determine how the drug and virus treatment affect the tumour density and spatiotemporal distribution.

5.2.2. Chemotherapy

Figure 7 depicts the fractional distribution of the chemotherapeutic drug in body tissue. Simulation results show that the drug concentration is highest inside the tissue and that the drug concentration is reduced with time. Initially, the fractional drug concentration is maximum outside the tumour and with time it circulates in the tumour and redistributes
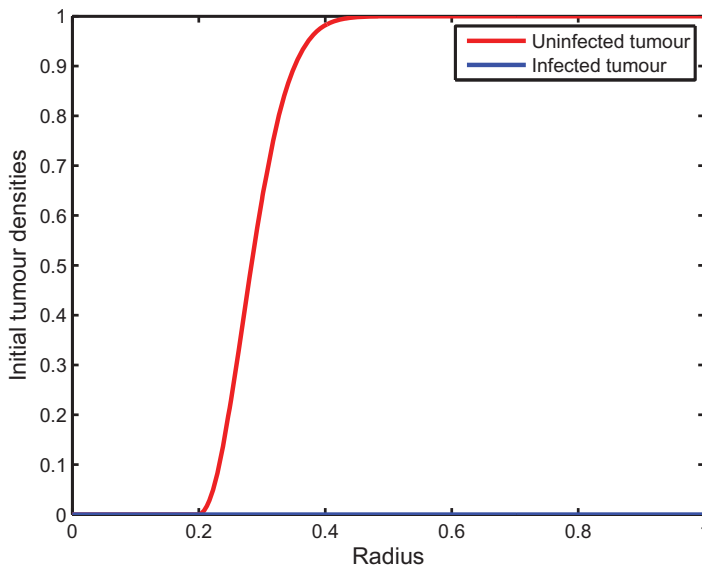
Figure 5. Initial fractional tumour cell densities. Uninfected tumour cells lie in the quiescent and proliferating zone $0.2 \leq r \leq 1$ while the region $0 \leq r \leq 0.2$ contains dead cells. The infected tumour density is initially zero in the whole domain.

to have a higher density inside the tissue, that it, maximum concentration is near the core than outside where $r \geq 0.2$.

Figure 8 (a–c) shows numerical solutions of Equation (7) which simulates the tumour with chemotherapy treatment. The tumour density in the tissue is reduced with time. When comparing the simulation results in Figures 6 and 8, we note that the tumour density was reduced from 0.849×10^6 to 0.790×10^6 cells per unit volume for a 10-day period treatment, from 0.998×10^6 to 0.41×10^6 cells per unit volume for a 25-day period treatment, and from 1×10^6 to 0.385×10^6 cells per unit volume for a 50-day period treatment. This reduction in tumour density is about 7%, 60% and 62% for the 10, 25, and the 50-day periods of treatment, respectively.

5.2.3. Virotherapy

Figure 9(a), (b), and (c) shows the numerical simulation of tumour treatment with virotherapy after 10, 25, and 50 days respectively. We notice that with time the virus reduces the uninfected tumour cell density from outside the tumour. Initially, we assume that there are no infected tumour cells in the tissue, that is $I = 0$, and the tumour has grown to maximum size. After a period of 10 days, Figure 9(a) shows that the infected tumour density begins to increase from outside the tissue, that is, $0.8 \leq r \leq 1$ and the uninfected tumour density begins to reduce throughout the tissue. After 25 days, the infected tumour density and the region in which it lies, increased to about 0.6×10^6 cells per unit volume in $0.6 \leq r \leq 1$. The uninfected tumour density was reduced to zero in this region. After 50 days, the infected tumour density occupied $0.2 \leq r \leq 0.6$, whereas the tumour density was reduced to zero in the region $0.4 \leq r \leq 1$.
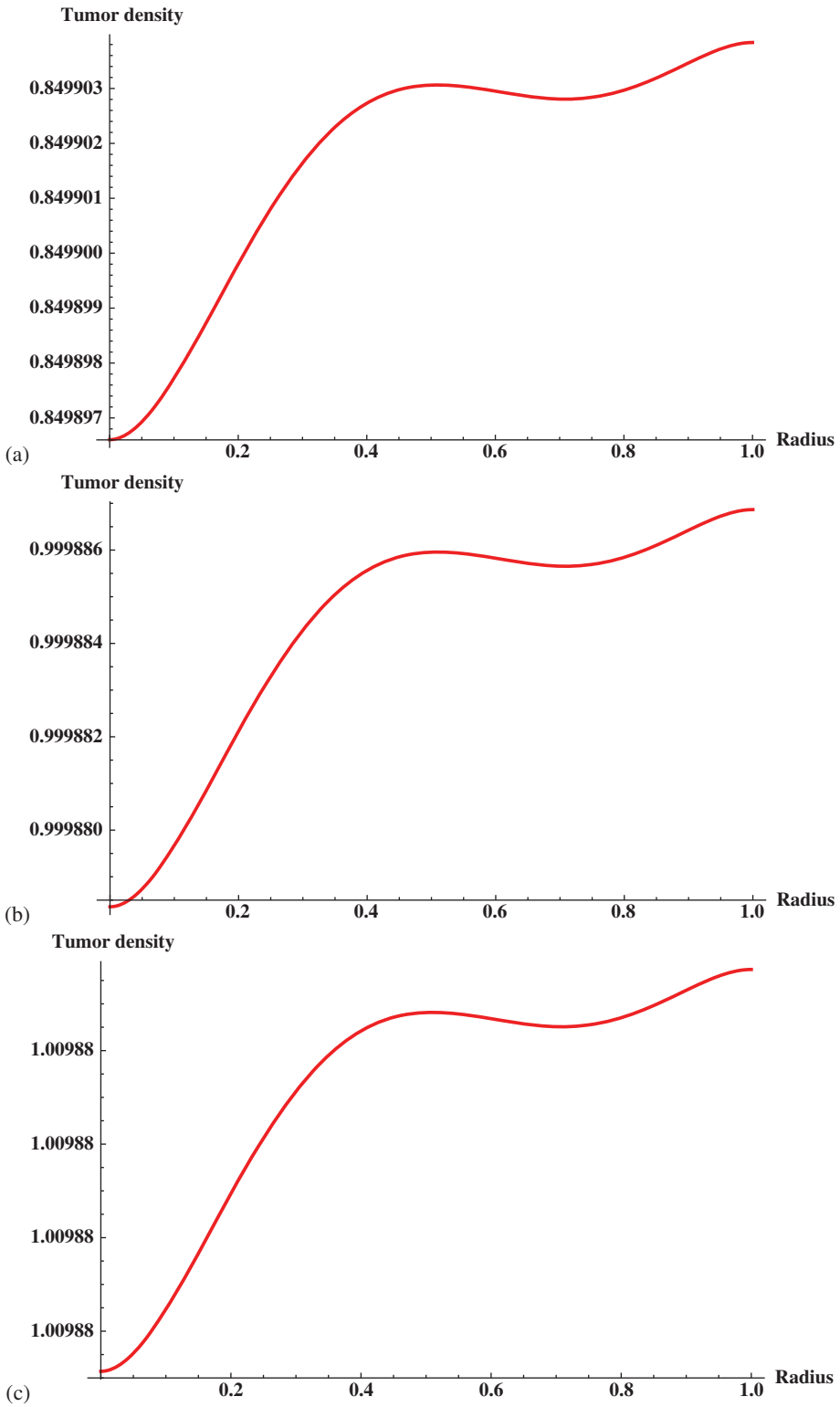
Figure 6. Spatial distribution of fractional untreated tumour density in the tissue at times corresponding to (a) 10, (b) 25 and (c) 50 days. The plots show that tumour density increases with time.
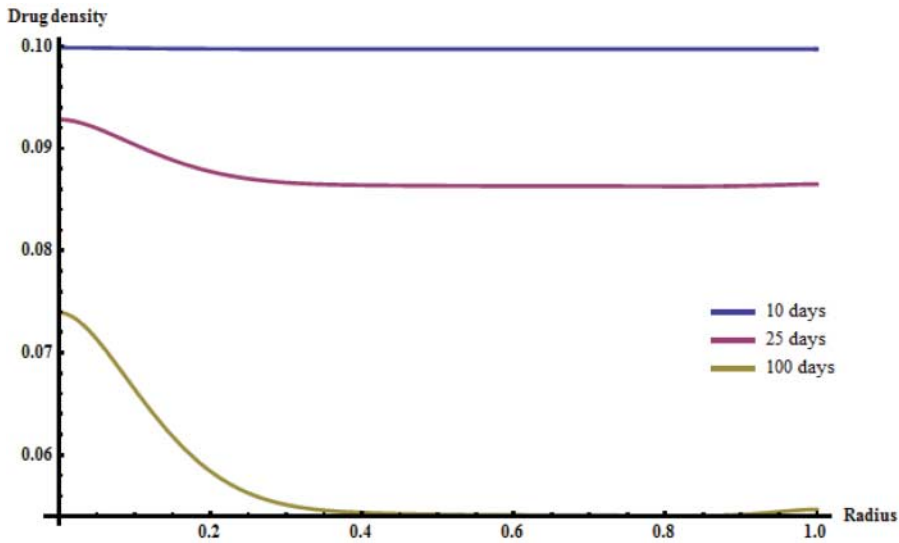
Figure 7. Simulation of Equation (10) showing distributions of the drug concentration for different time periods.

5.2.4. *Combining chemotherapy and virotherapy*

Figure 10 (a,b) shows the spatiotemporal dynamics of the tumour with both chemotherapy and virotherapy treatments combined. The simulation results are similar to those for virotherapy treatment except that the cell densities are reduced from both sides of the domain. The simulations indicate that with time, the tumour density reduces from both sides of the tissue domain, that is, from $r = 0$ and $r = 1$. After a 50-day period of treatment, the uninfected tumour density occupies a narrower domain, $0.2 \leq r \leq 0.8$, compared to the region, $0 \leq r \leq 1$, that it occupied after the 10-day treatment period. Simulation results show that, when both chemotherapy and virotherapy treatments are combined, the uninfected tumour density is reduced to a lower value compared to either chemotherapy or virotherapy treatments. For example, for the case of a 50-day period of treatment, we notice that: (a) with chemotherapy alone, in Figure 8(c), the uninfected density is about 0.41×10^6 in the whole tumour domain $0 \leq r \leq 1$, (b) with virotherapy alone, in Figure 9(c), the uninfected density is decreased from its highest peak of 0.9×10^6 to zero and lies in a reduced domain $0 \leq r \leq 0.4$, and (c) with chemotherapy and virotherapy combined, in Figure 10(c), the highest peak of the tumour is about 0.6×10^6 and lies in the region $0.2 \leq r \leq 0.7$. Going by the peak and the domain occupied by the cell densities, this means that combining chemotherapy and virotherapy results in about 20% improvement compared to virotherapy alone and about 37% compared to chemotherapy alone.

We further notice that the number of infected tumour cells is highly reduced with chemovirotherapy compared to treatment with virotherapy. For example, after a 50-day period of treatment with virotherapy alone, when comparing Figures 9(c) and 10(c) we notice that the infected tumour cells are 0.5×10^6 and lie in the region $0.2 \leq r \leq 0.6$, whereas with chemovirotherapy they are about 0.2×10^6 and covering $0.6 \leq r \leq 0.8$. That is about 80% difference between the two treatments. The simulations show that chemovirotherapy has a double-edged sword effect, with the ability to reduce tumour cells spatially
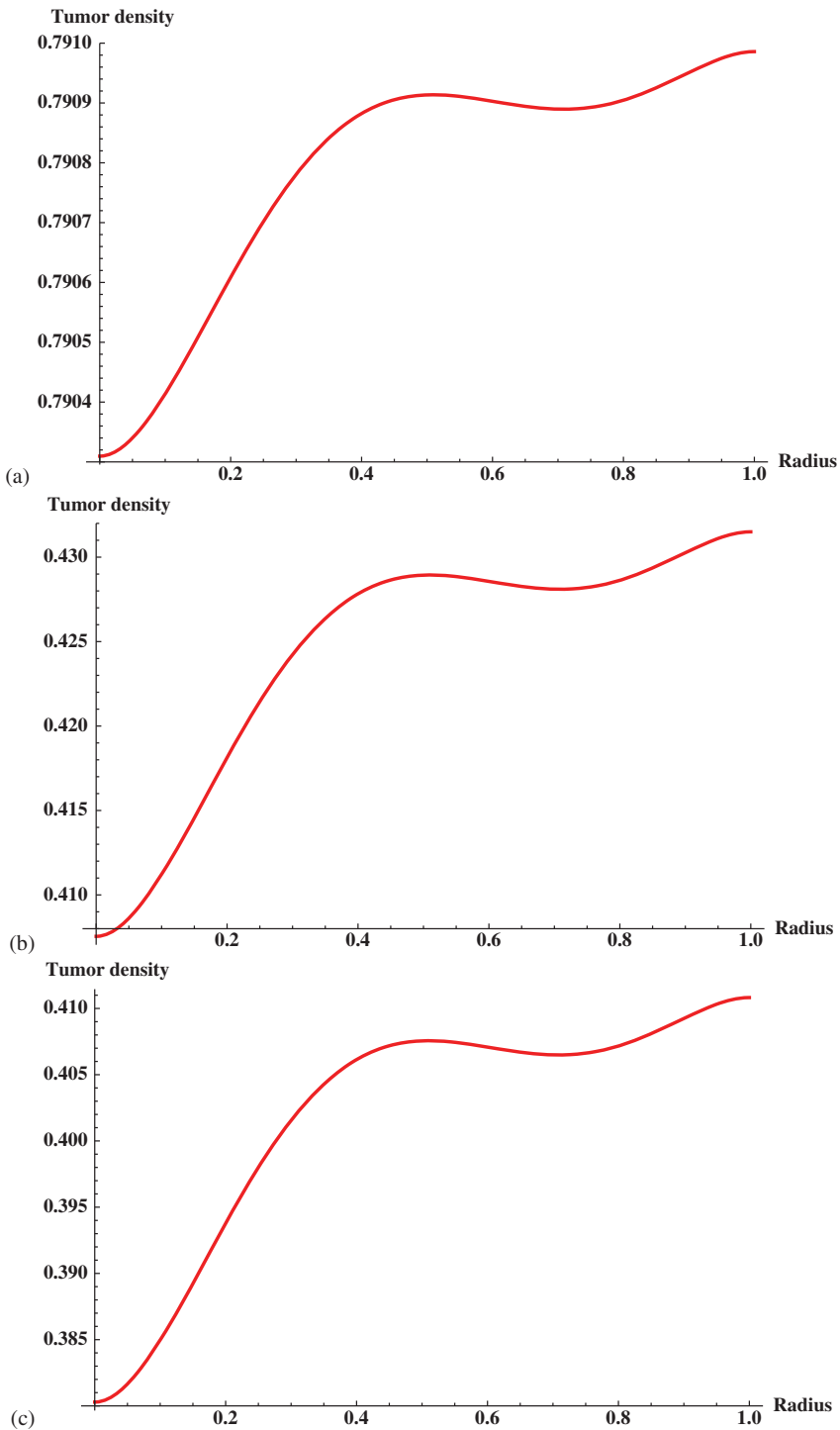
Figure 8. Chemotherapy alone: Spatial distribution of fractional tumour density in the tissue with chemotherapy treatment at times corresponding to (a) 10, (b) 25, and (c) 50 days. The plots show that the tumour density reducing with time.
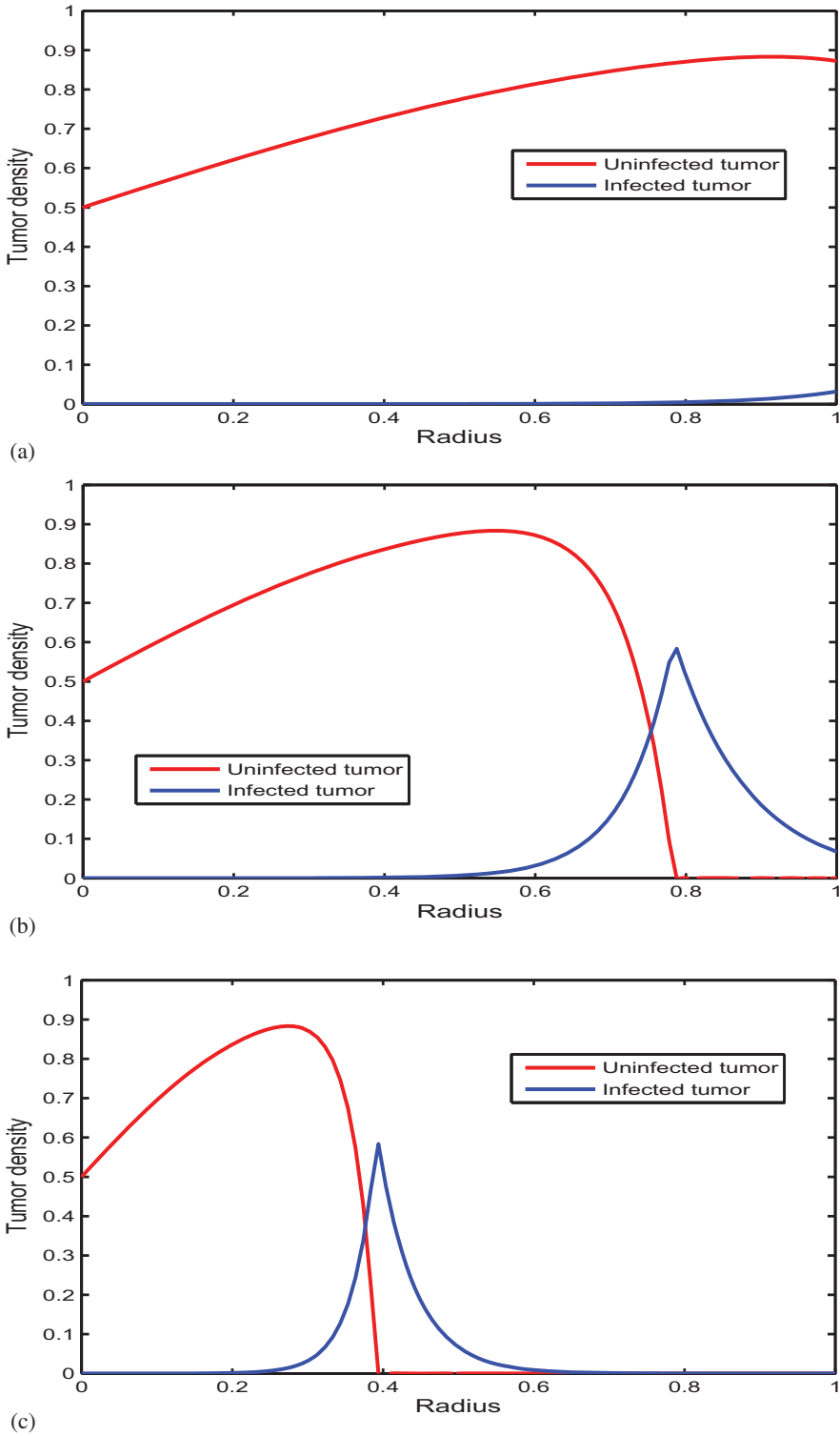
Figure 9. Virotherapy alone: Spatial distribution of fractional uninfected and infected tumour densities with virotherapy treatment for times corresponding to (a) 10, (b) 25, and (c) 50 days. Both infected and uninfected tumour densities begin to reduce from outside the tissue.
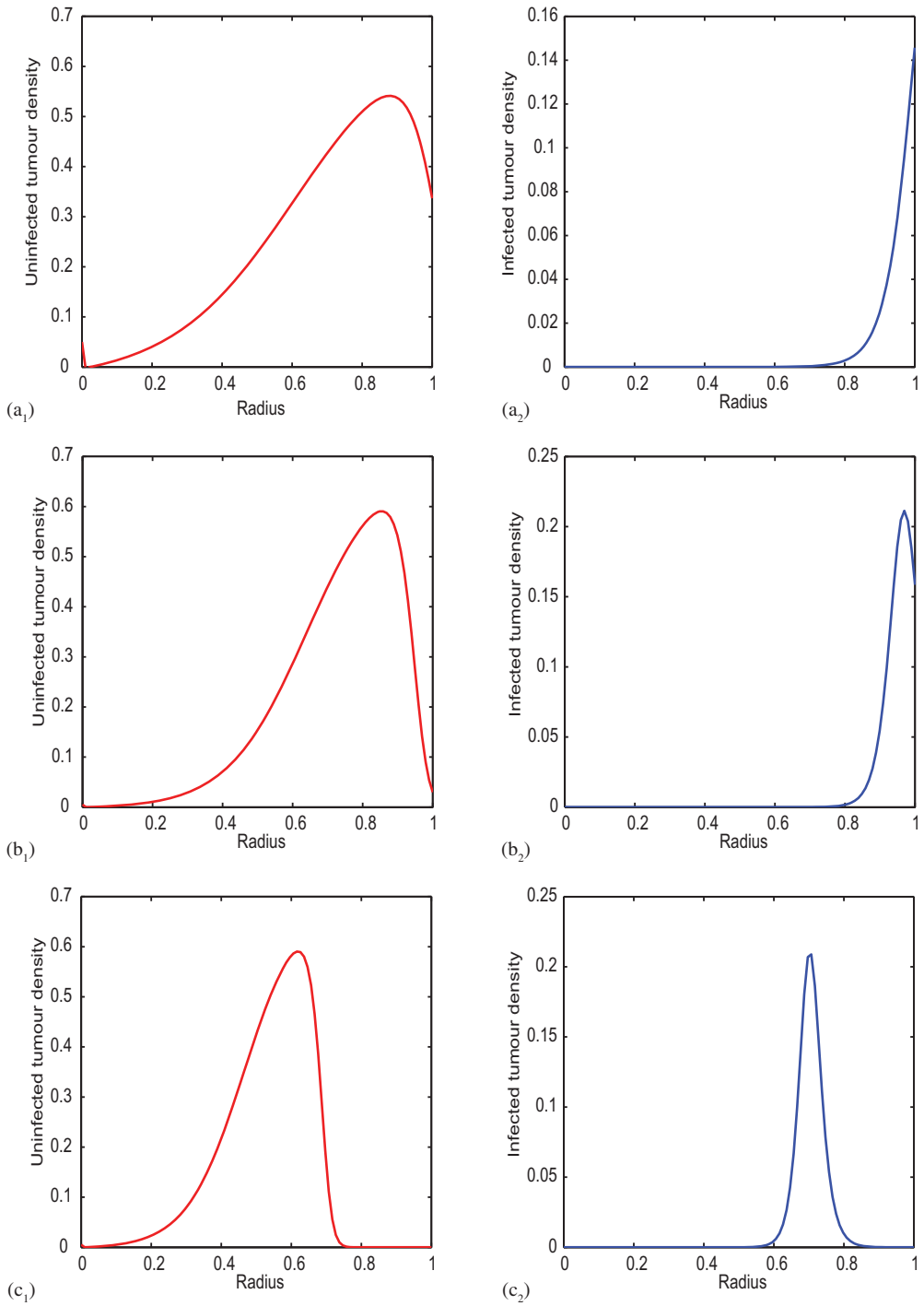
Figure 10. Combining chemotherapy and virotherapy: spatial distribution of fractional uninfected and infected tumour densities with both treatments for times corresponding to (a) 10, (b) 25, and (c) 50 days. The infected tumour density increases from outside the tissue and uninfected tumour density is reduced from both sides of body tissue.

throughout body tissue and in a small time period. The viruses infect and directly lyse tumour cells rendering them weaker and prone to lysis by the chemotherapeutic drug [1, 3, 52]. Moreover, the chemotherapeutic drug directly kills uninfected tumour cells as well.

These simulation results assert that combining chemotherapy and virotherapy to treat cancer is more effective and a good alternative to either chemotherapy or virotherapy alone, which is in agreement with the latest experimental studies [3, 6, 8, 12, 23, 24, 43, 45, 49, 61, 62]. These studies have shown that the right combination of oncolytic viruses and chemotherapy agents resulted in enhanced therapeutic effects not attainable by either therapy alone.

6. Uncertainty and sensitivity analysis

In this section, we study the dependence of the model solutions on the parameter values. In doing so, we are able to determine a feasible range of parameter values and ascertain the most critical parameters in the model. We employ two techniques which are discussed in detail by Marino et al. [38], that is, Latin hypercube sampling (LHS) for studying uncertainty analysis and partial rank correlation coefficient (PRCC) for calculating the sensitivity analysis indexes of the parameters. We ran the LHS/PRCC analysis with a sample size of 100. The choice of this sample size is due to the fact that PRCC produces accurate results for a lower sample size compared to other techniques like eFAST [38].

Uncertainty and sensitivity analysis were performed on all non-dimensional model parameters in the homogeneous model (13)–(16) with the aim of determining the most sensitive parameters to the model prediction of the cell densities. The parameter baseline values in Equation (22) were varied in the range of 25%. We considered the same initial cell densities as in the homogeneous model simulations. The indices were calculated at $t = 5$, a time just before all cell densities have reached equilibrium. Figure 11 displays a bar graph of PRCCs plotted against the homogeneous parameter values with the infected tumour density as the baseline dependent variable. The parameters which are significantly positively correlated with infected tumour cell density, at $p < 0.01$ level of significance, are tumour growth rate α and drug decay μ, while lysis-induced rate of tumour by the drug, δ_0, is significantly negatively correlated. An increase in the intrinsic production of tumour cells, α, leads to higher numbers of tumour cells, thus leading to an increase in the number of infected tumour cells. An increase in the drug decay, μ, leads to a less drug concentration in the body tissue, thus reducing the effect of the drug on the tumour cells and thereby leading to an increase in the number of infected tumour cells. The higher the drug lysis rate, δ_0, the lower the number of uninfected tumour cells, thus leading to a decrease in the number of tumour cells infected. Similarly, Figure 12 shows that the highest significantly correlated parameters with the virus density are virus burst size b which is positively correlated and lysis-induced rate of infected tumour by the drug δ_1 which is negatively correlated. An increase in the virus burst size implies an increase in the production of virus copies, thus increasing the virus density. On the other hand, an increase in the lysis rate of infected tumour leads to an increase in their death, resulting in a decrease in the number of virus copies made. Comparing Figures 11 and 12, we notice that b, δ_1, and ψ have the highest PRCCs and therefore possess a greater influence, compared to other parameters, in determining the infected and virus densities although their ranks differ. We notice that
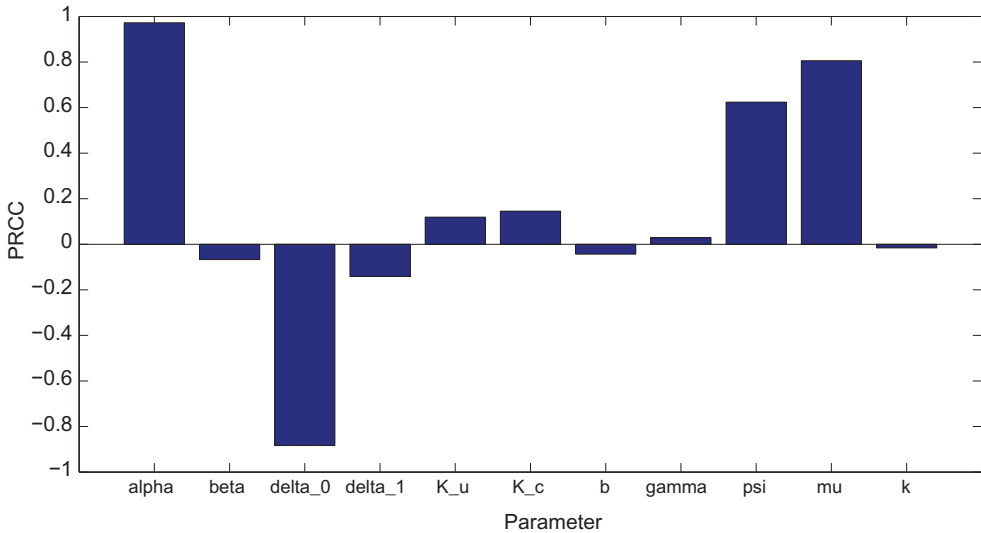
Figure 11. PRCCs of homogeneous model parameters with the infected cell density as the baseline variable and at the 5th day. All parameter values were varied in 25% of their baseline values in Table 1. The most sensitive parameters are shown to be α, δ_1, b, and ψ. The p-values of α, δ_1, δ_0, b, and ψ are all less than 0.002. Key: alpha $= \alpha$, beta $= \beta$, delta_0 $= \delta_0$, delta_1 $= \delta_1$, $k_u = K_u$, $k_c = K_c$ delta $= \delta$, gamma $= \gamma$, psi $= \psi$, and mu $= \mu$.

much as other parameter values, for example, the virus infection rate, β, have a significant p-value, they have less PRCCs, thus rendering them less sensitive to the model predictions compared to α, b, δ_0, δ_1, and ψ.

7. Discussion

In this paper, we developed a mathematical model of the spatiotemporal dynamics of chemovirotherapy treatment to cancer. Unique to this model is the inclusion of both chemotherapy drugs and virotherapy treatments, which has not been investigated before by means of mathematical modelling. The model describes an avascular solid tumour growth under chemovirotherapy treatment in spherical coordinates under the assumption of radial symmetry. We investigate the spatiotemporal distribution of infected and uninfected tumour cells as well as the outcome of chemovirotherapy treatments. We use the minimum wave speed of tumour invasion, numerical simulations, and sensitivity analysis to establish the key parameters that promote cancer remission during chemovirotherapy treatment.

The model was analysed in two main phases. First without the consideration of space and later with the inclusion of a space variable. The homogeneous model solution properties were investigated and a stability analysis was carried out on the steady-state solutions. A minimum wave speed of tumour invasion, in one dimension, was determined by converting the spatiotemporal model into a system of first-order ODEs and analysing its phase space. Numerical simulations for both temporal and spatiotemporal models were carried out using experimental data from the literature summarized in Table 1. A sensitivity
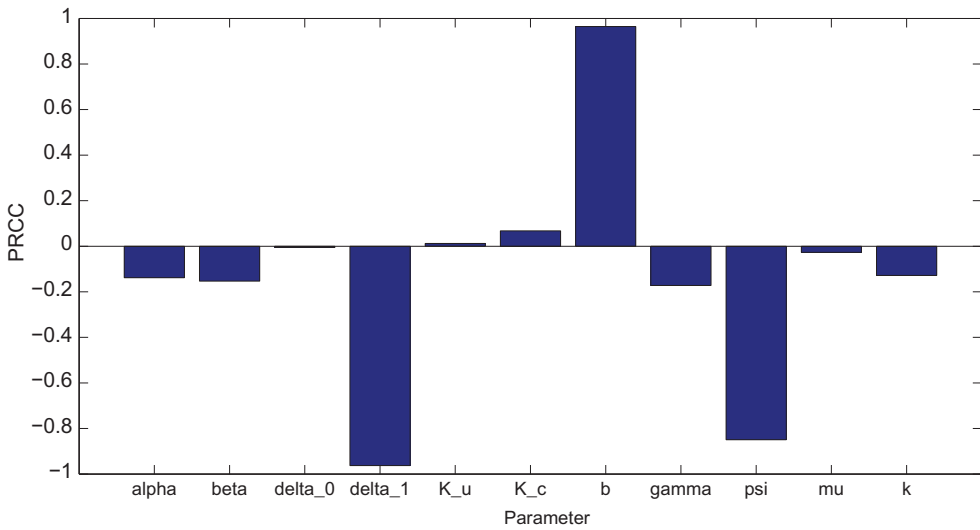
Figure 12. PRCCs of homogeneous model parameters with the virus density as the baseline variable ran at the 5th day. All parameter values were varied in 25% of their baseline values in Table 1. The bar graph shows δ_1, b, and ψ as the most sensitive. alpha $= \alpha$, beta $= \beta$, delta_0 $= \delta_0$, delta_1 $= \delta_1$, $k_u = K_u$, $k_c = K_c$ delta $= \delta$, gamma $= \gamma$, psi $= \psi$, and mu $= \mu$.

analysis was performed to identify critical parameters of the model. The main results obtained from this study are:

(1) Chemotherapy, alone, may not be able to clear all tumour cells from body tissue. This is depicted in Figure 2 which shows that even after 40 days, the tumour concentration was only reduced to its steady state.

(2) The virus burst size and infection rates are key factors in determining the success of the virotherapy treatment as was observed in Equation (21) that depicts the homogeneous model equilibriums. The homogeneous model analysis showed that high values of the virus burst size and the virus infection rate lead to lower tumour densities. This is in agreement with the mathematical studies by [13, 57].

(3) As shown in Figures 3 & 4 and 9 & 10, chemovirotherapy, as a form of cancer treatment, is more effective than chemotherapy and virotherapy treatments alone and is capable of eliminating tumour cells from body tissue in less than a week.

(4) The most critical parameters during chemovirotherapy according to travelling wave analysis in Section 5.1 are: tumour diffusivity and tumour growth rate. The most critical parameters in reference to sensitivity analysis in Section 6 are: virus burst size, tumour growth rate, drug lysis rates, and drug injection rate. Some of these parameters are as well depicted by the steady-state solutions in Section 4. Some of these parameters have already been identified as highly important for successful cancer treatment for in [13, 35, 57].

Despite the lack of longitudinal data for chemovirotherapy treatment, our analysis and numerical results are in agreement with latest clinical [6, 8, 51], experimental [60, 71], and mathematical studies [13, 25, 26, 36, 57] on virotherapy and chemovirotherapy. Tian

[57] affirms that tumour concentration can diminish to low undetectable cell counts provided that the burst size is large. Similarly, we have shown in the homogeneous case and sensitivity analysis that virus burst size and infection rates are critical in determining the outcome of virotherapy and chemovirotherapy treatments. It is worth noting that the larger the virus burst size, the higher the number of infected tumour cells, thus rendering them weak to progress and damage body tissue as shown in [57]. Crivelli et al. [13] assert that virus replication and virus-tumour cells fusion should be optimized in order to maximize virotherapy.

The mathematical model presented in this study considers a couple of simplifying assumptions and omits certain biological aspects during tumour invasion mainly the immune response which has been shown to impede tumour development [33, 37, 40]. Despite this fact, the results of this study affirm that combining chemotherapeutic drugs and viruses to treat cancer is more effective and a good alternative to either chemotherapy or virotherapy, which is in agreement with [6, 60]. The parameter sets, highlighted in this study, could be helpful in pointing out pertinent factors to consider in designing treatment protocols for chemovirotherapy treatment. The present model may be viewed as a stepping stone towards understanding the dynamics of chemovirotherapy treatment. This study can be extended to consider a higher spatial domain such as 3D to better describe the tumour geometry. A consideration of the tumour microenvironment, such as the extracellular matrix, would be a good extension of this study to investigate the effect of chemovirotherapy on normal body tissue cells. Our model is limited to a tumour that has grown to maximum size, prior to angiogenesis. Another plausible extension would be to model chemovirotherapy during the angiogenesis stage.

Disclosure statement

No potential conflict of interest was reported by the authors.

References

[1] M. Aghi, S. Rabkin, and R.L. Martuza, *Effect of chemotherapy-induced DNA repair on oncolytic herpes simplex viral replication*, J. Natl. Cancer Inst. 98 (2006), pp. 38–50.

[2] M. Al-Tameemi, M. Chaplain, and A. d'Onofrio, *Evasion of tumours from the control of the immune system: Consequences of brief encounters*, Biol. Direct 7 (2012), p. 1.

[3] M.M. Alonso, C. Gomez-Manzano, H. Jiang, N. Bekele, Y. Piao, W.K.A. Yung, R. Alemany, and J. Fueyo, *Combination of the oncolytic adenovirus icovir-5 with chemotherapy provides enhanced anti-glioma effect in vivo*, J. Cancer Gene Ther. 14 (2007), pp. 756–761.

[4] Ž. Bajzer, T. Carr, K. Josić, S.J. Russell, and D. Dingli, *Modeling of cancer virotherapy with recombinant measles viruses*, J. Theor. Biol. 252 (2008), pp. 109–122.

[5] S. Benzekry, C. Lamont, A. Beheshti, A. Tracz, J.M. Ebos, L. Hlatky, and P. Hahnfeldt, *Classical mathematical models for description and prediction of experimental tumor growth*, PLoS Comput. Biol. 10 (2014), p. e1003800.

[6] E. Binz, U. Lauer, E. Binz, and U.M. Lauer, *Chemovirotherapy: Combining chemotherapeutic treatment with oncolytic virotherapy*, J. Drug Design Dev. Therapy 9 (2015), pp. 1209–1216.

[7] G.J. Bosl and S. Patil, *Carboplatin in clinical stage I seminoma: Too much and too little at the same time*, J. Clin. Oncol. 29 (2011), pp. 949–952.

[8] S. Bossow, C. Grossardt, A. Temme, M. Leber, S. Sawall, E. Rieber, R. Cattaneo, C. von Kalle, and G. Ungerechts, *Armed and targeted measles virus for chemovirotherapy of pancreatic cancer*, J. Cancer Gene Ther. 18 (2011), pp. 598–608.

[9] T.D. Brock, *The emergence of bacterial genetics*, Cold Spring Harbor Laboratory Press Cold Spring Harbor, NY, 1990.

[10] L. Chahrazed and F.L. Rahmani, *Global stability and spatial spread of the nonlinear epidemic model*, Eur. Sci. J. 9 (2013).

[11] M.A.J. Chaplain, *Avascular growth, angiogenesis and vascular growth in solid tumours: The mathematical modelling of the stages of tumour development*, Math. Comput. Model. 23 (1996), pp. 47–87.

[12] J. Cody and D. Hurst, *Promising oncolytic agents for metastatic breast cancer treatment*, Oncolytic Virother. (2015), pp. 63–73.

[13] J.J. Crivelli, J. Földes, P.S. Kim, and J.R. Wares, *A mathematical model for cell cycle-specific cancer virotherapy*, J. Biol. Dyn. 6 (2012), pp. 104–120.

[14] V.L. de Rioja, N. Isern, and J. Fort, *A mathematical approach to virus therapy of glioblastomas*, Biol. Direct 11 (2016), p. 1.

[15] D. Dingli, K.W. Peng, M.E. Harvey, P.R. Greipp, M.K. O'Connor, R. Cattaneo, J.C. Morris, and S.J. Russell, *Image-guided radiovirotherapy for multiple myeloma using a recombinant measles virus expressing the thyroidal sodium iodide symporter*, Blood 103 (2004), pp. 1641–1646.

[16] M.L. Disis, *Immune regulation of cancer*, J. Clin. Oncol. 28 (2010), pp. 4531–4538.

[17] FDA: *FDA approves first of its kind product for the treatment of melanoma*, 2016. Available at http://www.fda.gov/NewsEvents/Newsroom/PressAnnouncements/ucm469571.htm (accessed September 6, 2016).

[18] FDA: *Time line of progress*, 2016. Available at http://www.cancerresearch.org/our-strategy-impact/timeline-of-progress/timeline-detail (accessed September 6, 2016).

[19] F.A. Fornari, J.K. Randolph, J.C. Yalowich, M.K. Ritke, and D.A. Gewirtz, *Interference by doxorubicin with DNA unwinding in MCF-7 breast tumor cells*, J. Mol. Pharmacol. 45 (1994), pp. 649–656.

[20] A. Friedman, J.P. Tian, G. Fulci, E.A. Chiocca, and J. Wang, *Glioma virotherapy: Effects of innate immune suppression and increased viral replication capacity*, Cancer Res. 66 (2006), pp. 2314–2319.

[21] K. Garber, *China approves world's first oncolytic virus therapy for cancer treatment*, J. Natl. Cancer Inst. 98 (2006), pp. 298–300.

[22] H.M. García-García, D. Goedhart, and P.W. Serruys, *Relation of plaque size to necrotic core in the three major coronary arteries in patients with acute coronary syndrome as determined by intravascular ultrasonic imaging radiofrequency*, Amer. J. Cardiol. 99 (2007), pp. 790–792.

[23] J.G. Gomez-Gutierrez, J. Nitz, R. Sharma, S.L. Wechman, E. Riedinger, E. Martinez-Jaramillo, H.S. Zhou, and K.M. McMasters, *Combined therapy of oncolytic adenovirus and temozolomide enhances lung cancer virotherapy in vitro and in vivo*, Virology 487 (2016), pp. 249–259.

[24] E. Hastie and V.Z. Grdzelishvili, *Vesicular stomatitis virus as a flexible platform for oncolytic virotherapy against cancer*, J. General Virol. 93 (2012), pp. 2529–2545.

[25] K. Jacobsen and S.S. Pilyugin, *Analysis of a mathematical model for tumor therapy with a fusogenic oncolytic virus*, Math. Biosci. 270 (2015), pp. 169–182.

[26] K.S. Kim, S. Kim, and I.H. Jung, *Dynamics of tumor virotherapy: A deterministic and stochastic model approach*, Stochastic Anal. Appl. 34 (2016), pp. 483–495.

[27] D. Kirschner and J.C. Panetta, *Modeling immunotherapy of the tumor–immune interaction*, J. Math. Biol. 37 (1998), pp. 235–252.

[28] N.L. Komarova and D. Wodarz, *Ode models for oncolytic virus dynamics*, J. Theor. Biol. 263 (2010), pp. 530–543.

[29] S.M. Larson, J.A. Carrasquillo, N.K.V. Cheung, and O.W. Press, *Radioimmunotherapy of human tumours*, Nat. Rev. Cancer 15 (2015), pp. 347–360.

[30] LLC: *European Commission Approves Amgen's IMLYGIC*^{TM} *(talimogene laherparepvec) As First Oncolytic Immunotherapy in Europe*, 2016. Available at http://immuno-oncologynews.com/2016/01/07/metastatic-melanoma-therapy-imlygic-now-available-eu/ (accessed October 4, 2016).

[31] W.X. Ma and B. Fuchssteiner, *Explicit and exact solutions to a Kolmogorov–Petrovskii–Piskunov equation*, Int. J. Non-Linear Mech. 31 (1996), pp. 329–338.

[32] H. Maeda, J. Wu, T. Sawa, Y. Matsumura, and K. Hori, *Tumor vascular permeability and the EPR effect in macromolecular therapeutics: A review*, J. Control. Release 65 (2000), pp. 271–284.

[33] K.J. Mahasa, R. Ouifki, A. Eladdadi, and L. de Pillis, *Mathematical model of tumor–immune surveillance*, J. Theor. Biol. 404 (2016), pp. 312–330.

[34] N.A. Maidana and H.M. Yang, *A spatial model to describe foot and mouth disease dissemination*. TEMA Tend. Mat. Apl. Comput. 12 (2011), pp. 11–20. doi:10.5540/tema.2011.012.01.0011.

[35] J. Malinzi, P. Sibanda, and H. Mambili-Mamboundou, Response of immunotherapy to tumour–TICLS interactions: A travelling wave analysis, Abstr. Appl. Anal. 2014 (2014). doi:10.1155/2014/137015.

[36] J. Malinzi, P. Sibanda, and H. Mambili-Mamboundou, *Analysis of virotherapy in solid tumor invasion*, J. Math. Biosci. 263 (2015), pp. 102–110.

[37] H. Mambili-Mamboundou, P. Sibanda, and J. Malinzi, *Effect of immunotherapy on the response of TICLs to solid tumour invasion*, J. Math. Biosci. 249 (2014), pp. 52–59.

[38] S. Marino, I.B. Hogue, C.J. Ray, and D.E. Kirschner, *A methodology for performing global uncertainty and sensitivity analysis in systems biology*, J. Theor. Biol. 254 (2008), pp. 178–196.

[39] J.L. Markman and S.L. Shiao, *Impact of the immune system and immunotherapy in colorectal cancer*, J. Gastrointest. Oncol. 6 (2014), pp. 208–223.

[40] A. Matzavinos, M.A. Chaplain, and V.A. Kuznetsov, *Mathematical modelling of the spatio-temporal response of cytotoxic t-lymphocytes to a solid tumour*, Math. Med. Biol. 21 (2004), pp. 1–34.

[41] K.M. Morrissey, T. Yuraszeck, C.C. Li, Y. Zhang, and S. Kasichayanula, *Immunotherapy and novel combinations in oncology: Current landscape, challenges, and opportunities*, Clin. Transl. Sci. 9 (2016), pp. 89–104.

[42] S. Motsa, *On a multi-domain bivariate Lagrange polynomial based spectral collocation method for solving non-linear evolution partial differential equations*, South African Symposium on Numerical and Applied Mathematics, University of Pretoria, 2015.

[43] A. Nguyen, L. Ho, and Y. Wan, *Chemotherapy and oncolytic virotherapy: Advanced tactics in the war against cancer*, Front. Oncol. 4 (2014). doi:10.3389/fonc.2014.00145

[44] R.T.D. Oliver, G.M. Mead, G.J. Rustin, J.K. Joffe, N. Aass, R. Coleman, R. Gabe, P. Pollock, and S.P. Stenning, *Randomized trial of carboplatin versus radiotherapy for stage I seminoma: Mature results on relapse and contralateral testis cancer rates in MRC TE19/EORTC 30982 study (ISRCTN27163214)*, J. Clin. Oncol. 29 (2011), pp. 957–962.

[45] K. Ottolino-Perry, J.S. Diallo, B.D. Lichty, J.C. Bell, and J.A. McCart, *Intelligent design: Combination therapy with oncolytic viruses*, Mol. Ther. 18 (2010), pp. 251–263.

[46] K.M. Page, *Mathematical modelling of tumour dormancy*, Math. Model. Nat. Phenomena 4 (2009), pp. 68–96.

[47] S. Pinho, D. Rodrigues, and P. Mancera, *A mathematical model of chemotherapy response to tumour growth*, Can. Appl. Math. Q. 19 (2011), pp. 369–384.

[48] I. Prigogine and R. Lefever, *Stability problems in cancer growth and nucleation*, Compar. Biochem. Physiol. Part B: Compar. Biochem. 67 (1980), pp. 389–393.

[49] K. Relph, H. Pandha, G. Simpson, A. Melcher, and K. Harrington, *Cancer immunotherapy via combining oncolytic virotherapy with chemotherapy: Recent advances*, Oncolytic Virother. 2016 (2016), pp. 1–13.

[50] B. Ribba, K. Marron, Z. Agur, T. Alarcón, and P. Maini, *A mathematical model of doxorubicin treatment efficacy for non-hodgkin's lymphoma: Investigation of the current protocol through theoretical modelling results*, Bull. Math. Biol. 67 (2005), pp. 79–99.

[51] D.R. Shafren, G.G. Au, T. Nguyen, N.G. Newcombe, E.S. Haley, L. Beagley, E.S. Johansson, P. Hersey, and R.D. Barry, *Systemic therapy of malignant human melanoma tumors by a common cold-producing enterovirus, coxsackievirus a21*, J. Clin. Cancer Res. 10 (2004), pp. 53–60.

[52] M. Siurala, S. Bramante, L. Vassilev, M. Hirvinen, S. Parviainen, S. Tähtinen, K. Guse, V. Cerullo, A. Kanerva, A. Kipar, M. Vähä-Koskela, and A. Hemminki, *Oncolytic adenovirus and doxorubicin-based chemotherapy results in synergistic antitumor activity against soft-tissue sarcoma*, Int. J. Cancer 136 (2015), pp. 945–954.

[53] R.D. Skeel and M. Berzins, *A method for the spatial discretization of parabolic equations in one space variable*, SIAM J. Sci. Stat. Comput. 11 (1990), pp. 1–32.

[54] J.S. Spratt, J.S. Meyer, and J.A. Spratt, *Rates of growth of human neoplasms: Part II*, J. Surg. Oncol. 61 (1996), pp. 68–83.

[55] I. Stamper, M. Owen, P. Maini, and H. Byrne, *Oscillatory dynamics in a model of vascular tumour growth-implications for chemotherapy*, Biol. Direct 5 (2010), p. 27.

[56] H.R. Thieme, *Mathematics in Population Biology*, Princeton University Press, Princeton, NJ, 2003.

[57] J.P. Tian, *The replicability of oncolytic virus: Defining conditions in tumor virotherapy*, Math. Biosci. Eng. 8 (2011), pp. 841–860.

[58] M.B. Tomblyn, M.J. Katin, and P.E. Wallner, *The new golden era for radioimmunotherapy: Not just for lymphomas anymore*, Cancer Control 20 (2013), pp. 60–71.

[59] Y. Touchefeu, P. Franken, and K.J. Harrington, *Radiovirotherapy: Principles and prospects in oncology*, Curr. Pharmaceut. Des. 18 (2012), pp. 3313–3320.

[60] S. Tusell Wennier, J. Liu, and G. McFadden, *Bugs and drugs: Oncolytic virotherapy in combination with chemotherapy*, J. Curr. Pharmaceut. Biotechnol. 13 (2012), pp. 1817–1833.

[61] I.V. Ulasov, A.M. Sonabend, S. Nandi, A. Khramtsov, Y. Han, and M.S. Lesniak, *Combination of adenoviral virotherapy and temozolomide chemotherapy eradicates malignant glioma through autophagic and apoptotic cell death in vivo*, Br. J. Cancer 100 (2009), pp. 1154–1164.

[62] G. Ungerechts, M.E. Frenzke, K.-C. Yaiw, T. Miest, P.B. Johnston, and R. Cattaneo, *Mantle cell lymphoma salvage regimen: Synergy between a reprogrammed oncolytic virus and two chemotherapeutics*, Gene Ther. 17 (2010), pp. 1506–1516.

[63] M. Vanneman and G. Dranoff, *Combining immunotherapy and targeted therapies in cancer treatment*, Nat. Rev. Cancer 12 (2012), pp. 237–251.

[64] J.G. Wagner, *Properties of the michaelis-menten equation and its integrated form which are useful in pharmacokinetics*, J. Pharmacokinet. Biopharm. 1 (1973), pp. 103–121.

[65] T. Wasil and S.M. Lichtman, *Clinical pharmacology issues relevant to the dosing and toxicity of chemotherapy drugs in the elderly*, Oncologist 10 (2005), pp. 602–612.

[66] H.L. Weber, M. Gidekel, S. Werbajh, E. Salvatierra, C. Rotondaro, L. Sganga, G.A. Haab, D.T. Curiel, E.G. Cafferata, and O.L. Podhajcer, *A novel CDC25B promoter-based oncolytic adenovirus inhibited growth of orthotopic human pancreatic tumors in different preclinical models*, Clin. Cancer Res. 21 (2015), pp. 1665–1674.

[67] L.M. Wein, J.T. Wu, and D.H. Kirn, *Validation and analysis of a mathematical model of a replication-competent oncolytic virus for cancer treatment implications for virus design and delivery*, Cancer Res. 63 (2003), pp. 1317–1324.

[68] D. Wodarz, *Computational modeling approaches to studying the dynamics of oncolytic viruses*, Math. Biosci. Eng. 10 (2013), pp. 939–957.

[69] D. Wodarz, *Computational modeling approaches to the dynamics of oncolytic viruses*, Wiley Interdiscip. Rev. Syst. Biol. Med. 8 (2016), pp. 242–252.

[70] D. Wodarz and N. Komarova, *Towards predictive computational models of oncolytic virus therapy: Basis for experimental validation and model selection*, PloS One 4 (2009), p. e4271.

[71] K. Zaoui, S. Bossow, C. Grossardt, M. Leber, C. Springfeld, P. Plinkert, C. von Kalle, and G. Ungerechts, *Chemovirotherapy for head and neck squamous cell carcinoma with EGFR-targeted and CD/UPRT-armed oncolytic measles virus*, J. Cancer Gene Therapy 19 (2012), pp. 181–191.